Available online at www.sciencedirect.com
SCIENCE DIRECT
Materials Research Bulletin 41 (2006) 1530–1542
Materials Research Bulletin
www.elsevier.com/locate/matresbu

Cation distribution, structure and magnetic properties of lithium manganese iron oxide spinel solid solutions

C. Wende [a], Kh. Olimov [b], H. Modrow [b], F.E. Wagner [c], H. Langbein [a,*]

[a] *Institute of Inorganic Chemistry, Dresden University of Technology, 01062 Dresden, Germany*
[b] *Institute of Physics, University of Bonn, 53115 Bonn, Germany*
[c] *Physics Department, Technical University of Munich, 85748 Garching, Germany*

Received 14 October 2005; received in revised form 9 January 2006; accepted 18 January 2006
Available online 7 February 2006

Abstract

Single phase cubic spinel compounds $Li_xMn_{1+x}Fe_{2-2x}O_4$ ($x = 0, \ldots, 1$) were obtained by thermal decomposition of freeze-dried formate solutions of appropriate composition. The samples were characterized by X-ray powder diffraction and Rietveld refinement, XANES, ^{57}Fe Mössbauer spectroscopy and magnetization measurements. The combination of these methods provides useful conclusions concerning the structure, cation distribution and properties of the spinel solid solutions. The $Li_xMn_{1+x}Fe_{2-2x}O_4$ samples contain Mn(II) and Mn(III) or Mn(III) and Mn(IV) for $x < 0.5$ or $x > 0.5$, respectively. With the increase of x the portion of Li ions occupying tetrahedral sites increases and becomes 100% at about $x = 4/7$. In spite of the preferred occupation of octahedral sites by manganese(III), the experimental results can only be explained by a partial occupation also of tetrahedral sites by Mn(III). An increase of M_S with the increase of x (expected for a preferred substitution of magnetic ions in tetrahedral sites by non-magnetic Li ions) is not observed. It should be prevented by the decreasing cooperative coupling effects due to the reduction of the iron content.

Keywords: A. Ceramics; C. XAFS; C. Mössbauer spectroscopy; C. X-ray diffraction; D. Magnetic properties

1. Introduction

The quasi-binary spinel compounds $MnFe_2O_4$, $Li_{0.5}Fe_{2.5}O_4$ and $LiMn_2O_4$ in the quaternary system Li–Mn–Fe–O were investigated intensively regarding their structure and properties. In the spinel structure $(A)[B_2]O_4$, the oxygen-ions form a cubic close packed array, in which the A-cations occupy one-eighth of the tetrahedral sites and the B-cations are distributed over one half of the octahedral positions. Since the 1950s attention was focussed on the ferrimagnetic spinel ferrites, because new applications, e.g. radio, television and microwave devices, needed materials with excellent magnetic properties [1]. Up to now, differently substituted ferrimagnetic manganese ferrites and lithium ferrites are used as controllable components in the microwave engineering, such as switches and circulators, and as cores of high-frequency inductors and transformers [2]. Paramagnetic $LiMn_2O_4$ and lithium manganese oxide defect spinels [3] as well as $Li_{1+\delta}Mn_{2-\delta}O_4$ ($0 \leq \delta \leq 0.33$; spinel structure) — Li_2MnO_3 (layered rocksalt structure) — composites [4] were investigated intensively in the last decades as promising cathode materials for rechargeable

* Corresponding author. Tel.: +49 351 463 34366; fax: +49 351 463 37287.
E-mail address: Hubert.Langbein@chemie.tu-dresden.de (H. Langbein).

0025-5408/$ – see front matter © 2006 Elsevier Ltd. All rights reserved.
doi:10.1016/j.materresbull.2006.01.016

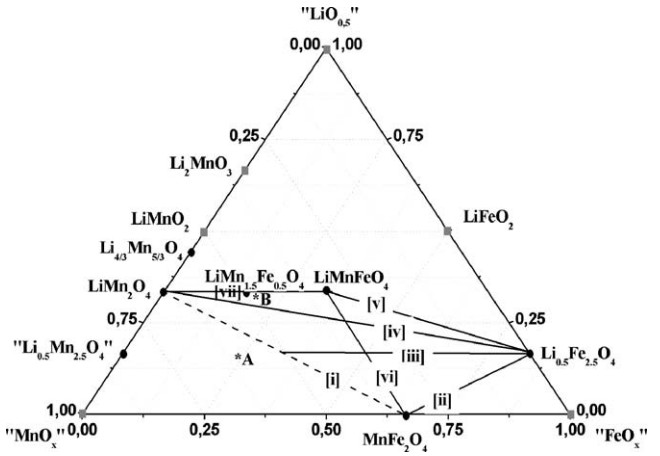

Fig. 1. Quasi-ternary phase diagram $LiO_{0.5}$–MnO_x–FeO_x as a projection on the Li–Mn–Fe-level showing well-known compounds and solid solutions [ii]–[vii] as well as the solid solution [i] investigated in this work.

lithium ion batteries. $MnFe_2O_4$ and $LiMn_2O_4$ are the end members of the solid solution series $Li_xMn_{1+x}Fe_{2-2x}O_4$ [i] investigated in this work (Fig. 1).

Manganese ferrite is a partially inverse spinel $(Mn_{1-\lambda}Fe_\lambda)[Mn_\lambda Fe_{2-\lambda}]O_4$ with the space group $F4_1/d\bar{3}2/m$ where λ is the degree of inversion. In $LiMn_2O_4$ the Mn^{3+} and Mn^{4+} ions are randomly distributed over the octahedral sites and the Li^+ ions occupy only tetrahedral sites. Lithium ferrite is an inverse spinel; contrarily to $LiMn_2O_4$, the lithium ions are located only on the octahedral sites according to the formula $(Fe)[Li_{0.5}Fe_{1.5}]O_4$. Above 755 °C, the Li^+ and Fe^{3+} ions are randomly distributed on the octahedral sites (space group $F4_1/d\bar{3}2/m$). Below 735 °C the face centered unit cell becomes primitive due to the 1:3 ordered distribution of the Li^+ and Fe^{3+} ions on the octahedral sites (space group $P4_332$) [5].

So far, only a few investigations have been carried out to study the cation distribution in the spinel-type Li–Mn–Fe oxides. Because of the relations between the cation distribution and the magnetic properties, this knowledge is important from a practical point of view. Petit and Lenglet [6] prepared $Li_{0.5-0.5x}Fe_{2.5-0.5x}Mn_xO_4$ ($0 \leq x \leq 1$) spinel solid solutions [ii] by reaction of mixtures of lithium ferrite and manganese ferrite at 850 °C in a vacuum ampoule. Independently of x, the Li^+ ions always occupy the B sites like in $(Fe)[Li_{0.5}Fe_{1.5}]O_4$. Spinels with $x \leq 0.2$ possess an 1:3 ordering of Li and Fe ions on the B sites and the Mn ions are only tetrahedrally coordinated. However, for $x > 0.2$ the Mn ions occupy both A and B sites, and a statistical distribution of the cations on the B sites was observed. The same order–disorder behaviour in dependence on x was also reported for the solid solutions $Li_{0.5}Fe_{2.5-x}Mn_xO_4$ [iii] [7], $Li_{1-0.5x}Fe_{2.5x}Mn_{2-2x}O_4$ [iv] [8] and$Li_{1-0.5x}Fe_{1.5x+1}Mn_{1-x}O_4$ [v] [9]. In all these cases the lithium ions are distributed over the A and B sites. Bonsdorf et al. [10] have also described the solid solution series $Li_{0.5}Fe_{2.5-x}Mn_xO_4$ [iii]. Contrary to [7] they found that the maximum x value for single phase spinels is $x = 1.5$ and for $x = 0.5$ the 1:3 cation order on the B sites is already completely destroyed. The composition with $x = 1.5$ was characterized by Mössbauer spectroscopy as $(Li_{0.5}Fe_{0.4}Mn_{0.1})[Fe_{0.6}Mn_{1.4}]O_4$ with Li ions only on the A sites of the spinel. Zakharov and Garbanov [11] and Shigemura et al. [12] have investigated sections with a continuous change of the valence state of manganese. In [11] the solid solutions $MnFe_2O_4$–$LiMnFeO_4$ [vi] were synthesized in air or oxygen atmosphere at 650–1300 °C. The authors assume that Mn(III) and Mn(IV) as well as Mn(II) exist side by side, e.g. $(Li_{0.16}Fe_{0.63}Mn_{0.21}{}^{2+})[Li_{0.34}Fe_{0.87}Mn_{0.58}{}^{3+}Mn_{0.21}{}^{4+}]O_4$. According to [12], solid solutions between $LiMn_2O_4$ and $LiMnFeO_4$ [vii] can be prepared at 600 °C in air. In these spinels only a small amount of lithium was found on the B sites.

From the above, it turns out that: (1) there is an order–disorder transition in solid solution spinels starting from lithium ferrite; (2) the cation distribution is influenced by the preparation conditions; (3) in Mn(II) and Fe(III) containing spinel compounds, the lithium ions have a preference to the B sites; with an increase of the content of Mn(III) and/or Mn(IV), which prefer the B sites, the lithium ions are located more and more on the A sites of the spinel.

Based on these conclusions, the main goal of the present work is to determine the cation distribution in $Li_xMn_{1+x}Fe_{2-2x}O_4$ spinel solid solutions and its correlation with various magnetic properties. According to an earlier publication [13], single phase spinels are formed throughout the whole range $0 \leq x \leq 1$, when special conditions of

Table 1
Synthesis parameters, oxidation number n of manganese, experimental and calculated M_S-values in Bohr magnetons and Curie temperature for selected single phase spinels $[Li_xMn_{1+x}Fe_{2-2x}O_4]_7$

Number	x	Sample	Synthesis condition		Mn^{n+}			M_S/μ_B at T		M_S/μ_B (calc.)	T_C (°C)
			T (°C)	$p(O_2)$ (atm)	n_{calc}	n_{XANES}	n_{chem}	5 K	300 K		
1	0	$Mn_7Fe_{14}O_{28}$	900	$N_2/H_2/H_2O/10^{-12}$	2.00	–	2.00	4.98	3.49		385
2	1/7	$Li_1Mn_8Fe_{12}O_{28}$	900	$N_2/10^{-3}$	2.38	–	2.35	4.03	2.51		300
3	2/7	$Li_2Mn_9Fe_{10}O_{28}$	900	Air	2.67	2.85	2.63	3.51	1.99	4.2	260
4	3/7	$Li_3Mn_{10}Fe_8O_{28}$	900	Air	2.90	2.94	2.89	3.48	1.78	5.15	–
5	1/2	$LiMn_3Fe_2O_8$[a]	900	Air	3.00	–	2.93	2.83[a]	1.26		93[a]
6	4/7	$Li_4Mn_{11}Fe_6O_{28}$	900	Air	3.09	3.17	3.14	2.52	0.75	6.32	55
7	5/7	$Li_5Mn_{12}Fe_4O_{28}$	900	O_2	3.25	–	3.24	1.33	0.00		–43
8	6/7	$Li_6Mn_{13}Fe_2O_{28}$	800	Air	3.38	3.34	3.41	0.17	0.00		–
9	1	$Li_7Mn_{14}O_{28}$	770	Air	3.50	–	3.48	0.00	0.00		–

n_{chem}: determined by chemical analysis; n_{XANES}: result of XANES; n_{calc}: calculated according to the second model (see text); M_S/μ_B (calc.): calculated values for the experimental determined compositions (see text); formula unit AB_2O_4.
[a] Values given in [10].

synthesis are used. Beside general information concerning the structure and phase composition, the X-ray powder diffraction including Rietveld structure refinement should give also special informations concerning the Li^+ ion distribution. XANES studies at the Mn and Fe K-edge should yield information on oxidation numbers of the cations and, in a qualified sense, on the site occupation. ^{57}Fe Mössbauer spectroscopy is a suitable method to determine the location of the Fe ions. A combination of these methods should allow useful conclusions concerning the investigated solid solution spinels. Taking into consideration results of other investigations, it should also allow some general conclusions concerning the Li–Fe–Mn–O-system as a whole.

2. Experimental procedure

The spinel compounds were obtained by thermal decomposition of freeze-dried formate solutions of appropriate composition as described elsewhere [13]. The experimental conditions for getting single phase spinels are shown in Table 1. For the determination of the average oxidation state the solid samples were dissolved together with a defined quantity of $(NH_4)_2Fe(SO_4)_2{\cdot}6H_2O$ in 50% sulfuric acid. Afterwards the Fe(III) formed by reaction of Mn(III) and/or Mn(IV) with Fe(II) was determined titrimetrically with cerium(IV) sulfate solution and Ferroin as indicator.

The phase analysis of the samples after thermal decomposition of the formate precursors was performed with a SIEMENS D5000 X-ray diffractometer (Cu Kα radiation; $10^\circ \leq 2\theta \leq 80^\circ$; step scan mode width 0.02°; 1 s per step). For quantitative statements the XRD data were collected in the 2θ range from 10° up to 140° in a step scan mode width 0.02° (6.7 s per step). Structure refinement was performed with the program WinPLOTR [14]. The background was interpolated because of a uneven background in the 2θ range between 10° and 20°. The Pseudo-Voigt function was used as peak shape model, sometimes an absorption factor for better B values.

Measurements of the saturation magnetization at 303 and 5 K were performed with a vibrating sample magnetometer (Oxford Instruments) and nickel as a calibration substance. The ac susceptibility was measured in the range of 30–400 °C and the Curie point was extrapolated from the obtained values.

X-ray absorption near edge structure (XANES) measurements of the selected samples of the solid solution series $Li_xMn_{1+x}Fe_{2-2x}O_4$ were carried out for both Mn and Fe K-edge at the beamline BN3 of the Electron Stretcher Accelerator (ELSA) at the University of Bonn, equipped with a modified Lemmonier-type double-crystal monochromator with Ge220 crystals [15]. The measurements were performed at 2.3 GeV electron energy in transmission mode. Ionization chambers were filled with air. Details on the experimental setup of this beamline can be found, e.g. in [16].

The energy range of the scan for Mn K-edge XANES measurements was from 6500 to 6700 eV in steps of 0.43 eV and 1000 ms integration time per step. For Fe K-edge XANES measurements the energy interval was from 7078 to 7250 eV with 0.52 eV step size and 1000 ms integration time per step. To extract the spectra, a linear background obtained by linear interpolation between two points in the pre-edge region of each spectrum was subtracted from the spectrum. The resulting XANES spectra were then normalized to 1 at 7200 eV for Fe K-edge data and at 6667 eV for

Mn K-edge data. To determine an average chemical shift, the position of the first inflection point was determined and correlated to a linear scale obtained from oxidic reference compounds with well defined formal valency.

In order to achieve a more detailed understanding of the sample system, Mn and Fe K-edge XANES spectra for different model compounds have been calculated using the FEFF8 code [17]. The reliability and amount of information which can be derived based on this type of calculation has been established for a broad variety of systems including solid state systems of varying complexity [18–21], nanoscaled systems [16,22,23] and metal-containing Fullerene modifications [24]. It should be mentioned that the code tends to underestimate the intensity of structures at the absorption edge, as discussed in detail in [18].

^{57}Fe Mössbauer spectra were taken with a ^{57}Co:Rh source at 295 and 4.2 K. At 4.2 K spectra were also taken with the absorber in a longitudinal external field of 6 T produced by a superconducting solenoid. The source was always at the same temperature as the absorber. For the measurement in the applied magnetic field the source was at a position where the field of the solenoid was negligibly small.

3. Results and discussions

3.1. Valence distribution and model selection, Rietveld refinement

A continuous series of single phase solid solution spinels $Li_xMn_{1+x}Fe_{2-2x}O_4$ throughout the range $0 \leq x \leq 1$ was synthesized. The experimental conditions are listed in Table 1. Fig. 2 shows the X-ray diffraction patterns of several samples with different compositions. All the diffraction patterns can be indexed in the cubic space group $F4_1/d\bar{3}2/m$. There are two different models to describe the cation distribution. According to [11] and taking into account the valence distribution of the end members of the solid solution series $(Mn^{2+})[Fe_2]O_4$ and $(Li)[Mn^{3+}Mn^{4+}]O_4$, a hypothetical model with Mn(III) and Mn(IV) ions in octahedral sites and Mn(II) ions in tetrahedral sites could be chosen. The general chemical formula for this model would be $Li_x{}^{+}Mn_{1-x}{}^{2+}Mn_x{}^{3+}Mn_x{}^{4+}Fe_{2-2x}{}^{3+}O_4$. In the second model, the average oxidation state of the manganese ions is obtained with contributions from only two different Mn ions according to $Li_x{}^{+}Mn_{1-2x}{}^{2+}Mn_{3x}{}^{3+}Fe_{2-2x}{}^{3+}O_4$ for $x \leq 0.5$ and $Li_x{}^{+}Mn_{2-x}{}^{3+}Mn_{2x-1}{}^{4+}Fe_{2-2x}{}^{3+}O_4$ for $0.5 \leq x \leq 1$. For both assumptions of the second model the Li ions can be: (a) distributed randomly over the A and B sites or (b) located on the A sites only. From the XANES measurements (see below) one finds that the spinel solid solutions contain Mn(II) and Mn(III) or Mn(III) and Mn(IV) only and the iron is mostly trivalent. The Mössbauer data also show that the iron is trivalent only. This is a proof for the second model.

The values of saturation magnetization M_S (Table 1) of the samples with a small degree of substitution allow the conclusion that lithium ions occupy both tetrahedral and octahedral sites (a). In case (b), for low degrees of substitution the M_S-values should increase with increasing lithium content in analogy to the well-known behaviour of manganese zinc ferrites [25]. A further indication for case (a) is the weak intensity of the (1 1 1)-diffraction peak for the samples

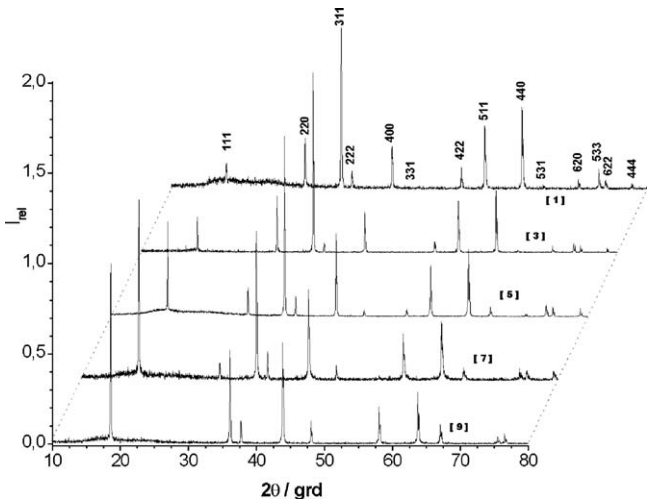

Fig. 2. XRD patterns of $Li_xMn_{1+x}Fe_{2-2x}O_4$; for sample numbers and synthesis conditions, c.f. Table 1.

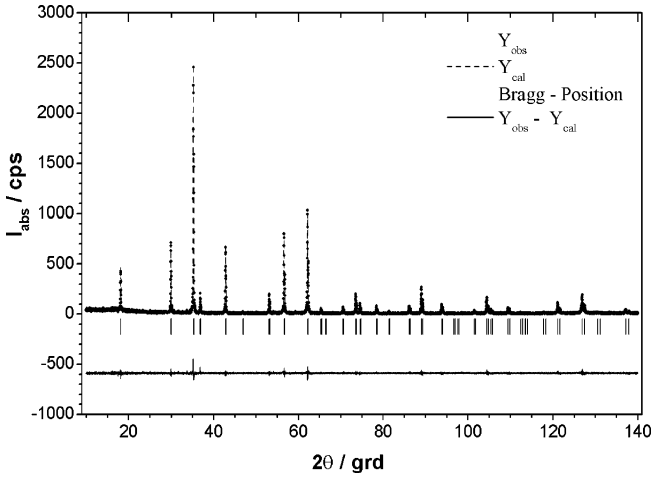

Fig. 3. Observed, calculated and difference plots resulting from the Rietveld analysis of the powder X-ray diffraction of $Li_xMn_{1+x}Fe_{2-2x}O_4$ ($x = 2/7$); structural parameters, c.f. Table 2.

with $x = 0, \ldots, 3/7$. A strong increase of the (1 1 1)-intensity and a decrease of the (2 2 0)-intensity especially for $x \geq 0.5$ indicate an increasing occupation of A sites by Li ions with an increase of x and perhaps a change in the general distribution of lithium ions at x values of about 0.5 to a strongly preferred occupation of only the A sites (Fig. 2). The same can be seen from the similar M_S values of samples with a middle degree of substitution. The experimental M_S values are the result of two competing effects: an increase of M_S with x because of a cation distribution according to (b) and a decrease of M_S because of the decrease of cooperative coupling.

The structure refinement by the Rietveld method was carried out for the whole range of the investigated solid solutions. The above-mentioned second model was chosen to determine the cation distribution over the octahedral (16d) and tetrahedral (8a) sites. For the calculation the well-known preference of Mn(III) and Mn(IV) to occupy octahedral sites and an occupation of tetrahedral holes by Mn(II) were assumed. Because of the good agreement between the calculated and the experimentally determined average valence states of manganese, the portions of manganese ions with different oxidation states were calculated from the theoretical average valence state. Together with the results concerning the Li occupation given above it seems to be possible that the true situation can roughly be described by the first case (a) for $x \leq 0.5$ and by the second mentioned cation distribution (b) for $x > 0.5$:

for $x \leq 0.5$ (a): $(Li_{x-\Delta}{}^{+}Mn_{1-2x}{}^{2+}Fe_{x+\Delta}{}^{3+})[Li_{\Delta}{}^{+}Mn_{3x}{}^{3+}Fe_{2-3x-\Delta}{}^{3+}]O_4$ with $0 < \Delta < x$, and

for $x > 0.5$ (b): $(Li_x{}^{+}Fe_{1-x}{}^{3+})[Mn_{2-x}{}^{3+}Mn_{2x-1}{}^{4+}Fe_{1-x}{}^{3+}]O_4$.

Fig. 3 shows the observed, calculated and difference profiles for one member of the series ($x = 2/7$). Table 2 gives the structural and cell parameters, the cation distribution, the thermal parameter as well as few final R factors and the goodness of fit, S^2, for the whole range of the solid solutions. The results given in Table 2 take into account that no exact conclusions concerning the site occupation of Mn(II), Mn(III), Mn(IV) and Fe(III) ions can be drawn from the XRD pattern and the refinement results. As a tetravalent ion, Mn(IV) should occupy only octahedral sites. This is taken into account in Table 2. Further information concerning the site occupation by Mn(II), Mn(III) and Fe(III) ions can be obtained by the Mössbauer and EXAFS experiments (see below). The Rietveld refinement only allows clear conclusions concerning the distribution of Li^+ ions over octahedral and tetrahedral sites.

One sees that with an increase of the amount of Mn(III) the lithium ion fraction on the tetrahedral sites is increased. That means that the Mn(III) ions move lithium from the B to the A sites. At degrees of substitution >3/7, practically all the lithium ions occupy tetrahedral sites. For samples with $x \geq 4/7$ the final R values and the square of the goodness of fit, S^2, are increased already for small portions of Li ions on octahedral sites. The compound with $x = 5/7$ seems to be an exception. It shows better R factors for a small amount of lithium on the octahedral sites, which would agree with the results of [12] for $LiMn_{1+x}Fe_{1-x}O_4$ solid solutions. But the generally worse agreement factors and the higher deviation in the lattice parameter indicate that in this case two similar spinel phases with slightly different

Table 2
Structural parameters for x $LiMn_2O_4 \cdot (1-x)MnFe_2O_4$ resulting from the Rietveld refinement in the space group $Fd\bar{3}m$

	Sample							
	$Mn_7Fe_{14}O_{28}$	$Li_1Mn_8Fe_{12}O_{28}$	$Li_2Mn_9Fe_{10}O_{28}$	$Li_3Mn_{10}Fe_8O_{28}$	$Li_4Mn_{11}Fe_6O_{28}$	$Li_5Mn_{12}Fe_4O_{28}$	$Li_6Mn_{13}Fe_2O_{28}$	$Li_7Mn_{14}O_{28}$
a (Å)	8.51260 ± 0.0001	8.47685 ± 0.0001	8.43702 ± 0.0001	8.42199 ± 0.0001	8.38681 ± 0.0001	8.35391 ± 0.0003	8.28476 ± 0.0002	8.24726 ± 0.0001
Oxygen parameter, u (Å)	0.25619(41)	0.25890(32)	0.25833(34)	0.25978(28)	0.26249(21)	0.26084(30)	0.26184(21)	0.26122(26)
Occupation on octahedral								
Fe^{3+}, Mn^{3+}, (Mn^{2+})	14	13.19	13.04	13.37	13	11.72	9	7
Mn^{4+}	–	–	–	–	1	3	5	7
Li^+	–	0.81	0.96	0.63	–	0.28	–	–
Occupational on tetrahedral								
Fe^{3+}, Mn^{2+}, (Mn^{3+})	7	6.81	5.96	4.63	3	2.28	1	–
Li^+	–	0.19(19%)	1.04(52%)	2.37(79%)	4(100%)	4.72(94.4%)	6(100%)	7 (100%)
Thermal parameter (Å)^2								
B (O^{2-})	1.561(13)	1.509(89)	1.496(91)	1.572(85)	1.736(78)	2.814(12)	1.756(74)	1.738(87)
B (octahedral)	1.034(67)	0.695(34)	0.660(34)	0.722(30)	0.982(25)	1.097(40)	0.701(22)	0.632(27)
B (tetrahedral)	0.952(89)	0.520(40)	0.757(47)	0.877(56)	1.037(56)	1.575(17)	1.948(154)	0.917(35)
Agreement factors								
R_p (%)	7.89	13.10	13.30	12.50	11.40	13.80	13.00	12.80
R_{wp} (%)	12.00	21.40	21.50	19.30	17.90	21.00	19.30	20.20
R_{exp} (%)	9.53	17.20	18.73	16.28	15.92	17.83	16.50	15.77
S^2_{weight}	2.44	1.87	2.11	2.79	1.67	1.69	1.52	2.44
R_B	4.22	3.53	4.77	4.01	4.24	6.19	3.66	4.90
R_F	3.00	3.87	3.74	2.79	3.88	5.67	3.70	4.11

compositions coexist. According to [13] the reaction seems to succeed only in a very narrow $p(O_2)$–T–area and at the chosen conditions are at best near the required ones.

One observes that with increasing lithium content the lattice constant decreases and the oxygen parameter (x, y, z) tends to increase. This is particularly obvious if Mn(II) is replaced completely by Mn(III) and Mn(IV). It can be explained by an increasing occupation of the tetrahedral A sites by the lithium ions with a relatively large ionic radius and a small charge-to-radius ratio. The increase of the oxygen parameter is caused by an enlargement of the tetrahedral holes and, with that, an increase of the A–O distance. This compensates the decrease of the A–O distance with the observed decrease of the lattice constant a. Besides, a gradual increase of the thermal parameter B for the A sites is observed. It can also be explained by the increase of the lithium ion occupation. According to [26], the influence of the lithium ions on the B sites is substantially smaller.

First of all, the preferred occupation of A sites by lithium ions in presence of a relatively large amount of Fe^{3+} ions on B sites is surprising. But, the site occupation in spinels is the result of some different and contrary influences. One might expect that, analogously to the inverse spinel $LiFe_5O_8$, the smaller Fe^{3+} ions prefer to occupy the smaller tetrahedral sites and the relatively large Li^+ ions prefer the larger octahedral sites. But, the electronic configuration of Li^+ is more favorable for tetrahedral bonding to the oxygen ions and the electrostatic Madelung energy of the spinel lattice favours the occupation of octahedral sites by ions with higher positive charge. With an oxygen parameter larger than the ideal value of 0.25, this ''normal arrangement'' of the metal ions will be energetically even more favourable. Because of the comparatively large Mn^{2+} ions, the oxygen parameter of manganese ferrite is already larger than the ideal value. This should explain the preferred occupation of tetrahedral sites by Li^+ ions in $Li_xMn_{1+x}Fe_{2-2x}O_4$ compounds already at small x values.

3.2. XANES results

Fig. 4a displays the Mn K-edge XANES spectra for selected members of the solid solution series $Li_xMn_{1+x}Fe_{2-2x}O_4$ as well as for a series on Mn oxides used as reference compounds. One can clearly see from Fig. 4a that the main edge positions (determined as discussed in the experimental section) of the samples under investigation are shifted relative to each other. To correlate this shift to a shift in formal valency, the edge shifts of reference oxides MnO, Mn_2O_3, and MnO_2 with the corresponding valencies 2+, 3+, and 4+ were fit with a linear model, as displayed in Fig. 5a. The valences of the spinel oxides were determined from their edge shifts using this curve as calibration. The values obtained in this way agree well with the theoretical values and the results of the wet chemical analysis, as shown in Table 1. A similar analysis is possible for the Fe K-edge data shown in Fig. 4b. Using the same approach for the assignment of an averaged formal valency, one obtains the results displayed in Fig. 5b, indicating clearly that the obtained value is close to three in all cases.

A more detailed comparison of the Mn K- edge spectral features of the reference oxides and the obtained data for the samples provides some additional information on the charge distribution. It is, for instance, possible to exclude that Mn^{4+} contributes in samples 3 and 4 (sample number see Table 1), because in their spectra no peak contributions in the white line region of the Mn^{4+} reference MnO_2 are found. Additionally, the shape resonance located at about 6575 eV in the MnO_2 reference spectrum, which creates a second maximum, does not lead to a clear maximum at this position in the spectra of samples 3 and 4. In contrast to that, both features are developed strongly in sample 8 and slightly in sample 6. Conversely, it is quite evident for sample 8 that the onset of absorption does not agree to the energy position which corresponds to the presence of Mn^{2+} as defined by the MnO reference, and the respective white line position of the reference does not match the position observed for sample 8. Whereas the onset of absorption cannot exclude the presence of Mn^{2+} in sample 6, the notable reduction of intensity as well as the energy shift in the white line region seems to suggest that Mn^{2+} is not present or at least strongly suppressed in this sample. Consequently, a fingerprint comparison suggests that only two valencies of Mn, 2+/3+ and 3+/4+, respectively, occur simultaneously in these samples, indicating that the second model discussed above is correct.

In contrast to the situation at the Mn K-edge, the identical approach at the Fe K-edge yields significantly less additional information. Clearly, the onset of absorption of the Fe_3O_4 reference is at lower energies than the one observed for any of the samples. Just as clearly, the energy position of the shape resonance at 7150 eV corresponds exactly with the one found in the Fe^{3+} reference. Consequently, all samples should contain exclusively Fe^{3+}.

However, the rich structural features of the spectra allow for an even more detailed description of the site occupation encountered in the solid solution samples than the mere determination of an average formal valency of the absorbing element and how this can be realized in terms of valence distribution. Returning to Fig. 4a, one observes that

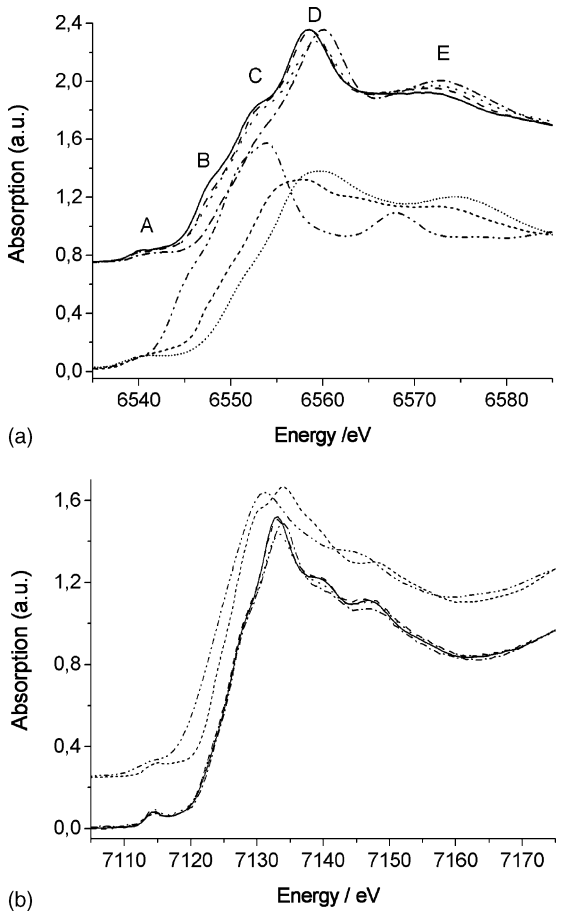

Fig. 4. (a) Experimental Mn K-edge XANES spectra of samples 3 (solid line), 4 (dashes), 6 (dots) and 8 (dashes and dots) and reference spectra of MnO (dashes and double dots), Mn_2O_3 (short dashes) and MnO_2 (short dots). (b) Experimental Fe K-edge XANES spectra of samples 3 (solid line), 4 (dashes), 6 (dots) and 8 (dashes and dots) and reference spectra of magnetite (dashes and double dots) and hematite (short dashes) (sample number see Table 1).

the general structure of the Mn K-edge spectra is equal for all samples under investigation—it shows five characteristic features: a pre-edge structure A, two shoulders B and C in the rising absorption edge, a pronounced maximum D and a strong shape resonance E. Both the intensity and the exact energy position of these features vary individually as a function of Li and Mn site occupation and Li content. The electronic structure observed at the Fe K-edge is quite similar to the case of the Mn spectra: a pre-edge structure A, two shoulders B and C in the rising edge and the pronounced white line D, but in contrast to the data, two shape resonances E and F are observed. The most significant change observed in the structures at the Fe K-edge is a shift of the white line position towards higher energy with higher Li-content.

In order to correlate the observed spectral changes to the variations in site occupation for the individual samples, FEFF8 [17] calculations have been performed on different model structures in the $Fd\bar{3}m$ space group, simulating the effects of complete Li substitution on the octahedral and tetrahedral cation sites on the XANES spectra of Fe and Mn atoms on tetrahedral and octahedral sites, respectively. This approach exaggerates the effects encountered in the actual system, making it well suited to illustrate the specific trends for different substitutions in the lattice most clearly, but unsuited for the exact reproduction of the spectra. It should also be noted that the massive substitutions naturally influence the position of the Fermi level in the model systems, therefore a stringent interpretation of the intensity and energy position of the pre-edge feature based on the model calculations has not been performed. Results of these model calculations are displayed in Fig. 6 and allow to investigate the spectral changes induced by three effects: The site distribution of the absorbing Fe and/or Mn atoms as well as both total Li content and Li site distribution. As shown

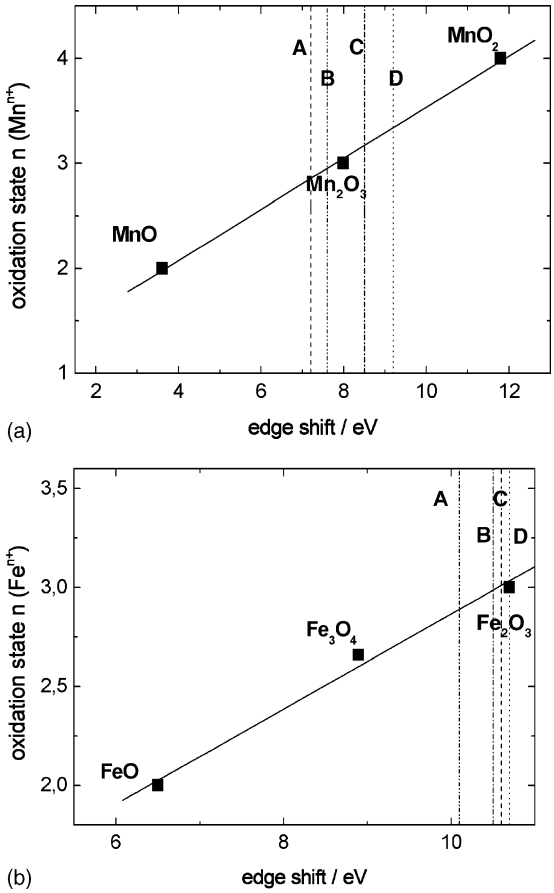

Fig. 5. (a) Calculation of average oxidation states (Mn^{n+}): sample 3 (+2.85) (A), sample 4 (+2.94) (B), sample 6 (+3.17) (C) and sample 8 (+3.34) (D). (b) Calculation of average oxidation states (Fe^{n+}): sample 4 (+2.89) (A), sample 6 (+2.96) (B), sample 3 (+2.98) (C) and sample 8 (+3.00) (D).

in Fig. 6a, the site which is occupied by the absorbing atom influences the spectrum characteristically, whereas differences between Mn and Fe absorbers are in general small. On octahedral sites, the white line intensity is much higher than on tetrahedral ones. In contrast to that, tetrahedral sites show more structured pre-edge features, especially more intense structures B and C on the rising absorption edge and a splitting of the white line.

In general, the addition of Li leads to a shift of the white line to higher energy (c.f. Fig. 6b and c) for absorber atoms located on either site. This observation meets the general expectation, as Li can only donate one charge and consequently the surrounding oxygen atoms reduce the electron population at the absorber metal sites more strongly. Analyzing the case for the absorbing atom on a tetrahedral site in more detail (c.f. Fig. 6b), one finds a more pronounced change of the position of the entire white line if the Li occupies the smaller tetrahedral site with a partially covalent character of the Li–O bonds. Instead, when Li is occupying the larger octahedral sites only, all energy positions remain nearly stationary, but the intensity of pre-edge peak A, the shoulder B and the (experimentally not resolved) post-white line structure changes notably. Tentatively, these changes can be correlated to the significantly smaller overlap of Li and O orbitals for Li on octahedral sites and the more ionic character of these Li–O bonds. This leads to some reconfigurations of the neighbouring Mn–O bonds, which is visible in the slightly changed intensity of the described absorption features.

For absorber atoms on octahedral sites (Fig. 6c), in general much smaller effects are observed, although the trend of a shift to higher energies is conserved, e.g. when analysing the onset of the absorption edge. The reduction of the drastic difference between Li on tetrahedral and octahedral sites in this case is tentatively assigned to the fact that the larger coordination number of the octahedral site leads to an increased stabilization of the electronic structure of the absorber atom.

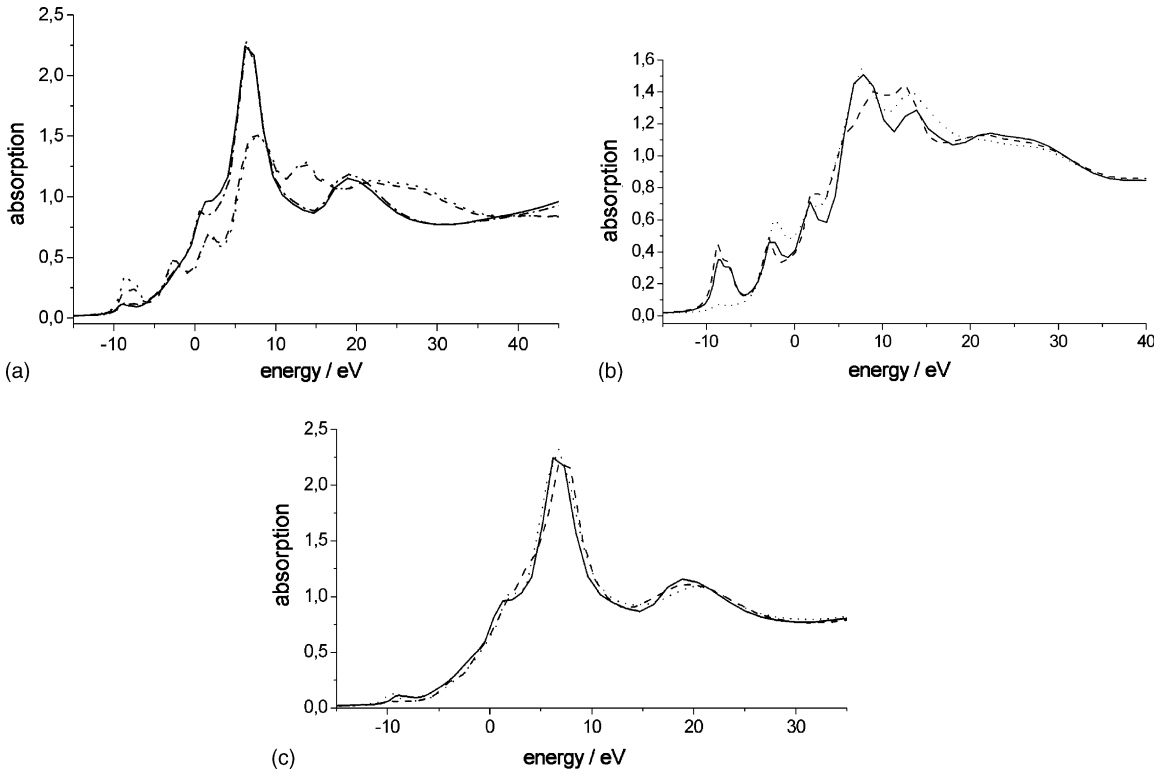

Fig. 6. (a) FEFF8 model calculations for: octahedral site absorber Mn, Mn on all cation sites (solid line); octahedral site absorber Fe, Fe on all cation sites (dashes and dots); tetrahedral site absorber Mn, Mn on all cation sites (dots); tetrahedral site absorber Fe, Fe on all cation sites (dashes). (b) FEFF8 model calculation for tetrahedral site absorber Mn: Mn on all cation sites (solid line); Li on all remaining tetrahedral cation sites, Mn on all octahedral cation sites (dashes); Mn on all remaining tetrahedral cation sites, Li on all octahedral sites (dots). (c) FEFF8 model calculation for octahedral site absorber Mn: Mn on all cation sites (solid line); Li on all remaining octahedral cation sites, Mn on all tetrahedral cation sites (dashes); Mn on all remaining octahedral cation sites, Li on all tetrahedral sites (dots).

Using these results, it is possible to interpret the changes in the Mn K-edge XANES spectra in terms of the proposed site occupation. The systematic reduction of intensity of structure B observed in samples 4, 6 and 8 clearly reflects the reduction of the relative amount on Mn on tetrahedral sites. At the same time, the notable contrast between the change in intensity for structures B and the smaller change in intensity observed for structure C when comparing the spectra of samples 3 and 4, respectively, confirms nicely the predicted preferred Li-occupation of the tetrahedral site in sample 4, as this should effect an increase of intensity of structure C for the remaining Mn atoms on tetrahedral sites. Also, the calculations verify the observed trend that the energy position of the white line is a function of Li-content.

At the Fe K-edge, the decreasing white line intensity of the spectra apparently reflects the reduction of the relative overhead of Fe located on octahedral sites. At the same time, the shift on the position of the white line can be related to an increasing amount of Li on tetrahedral sites, which is also suited to explain the reduction of the intensity of the shape resonances at about 7140 and 7148 eV, respectively.

3.3. Mössbauer spectra

The Mössbauer spectra confirm that all the iron in all samples is trivalent. The relative distribution of Fe over A and B sites was determined from the area ratio of the sextets due to Fe on A and B sites in the Mössbauer spectra taken at 4.2 K in an external magnetic field of 6 T (Fig. 7b), where the A and B sites are clearly distinguishable since for the A sites the external field is parallel to the hyperfine field, while the two fields are antiparallel for the B sites. The results are summarized in Table 3. Taking into account the results of the Rietveld refinements (Li^+ ion distribution, see Table 2) and chemical analyses as well as XANES-investigations (average oxidation number of manganese and iron

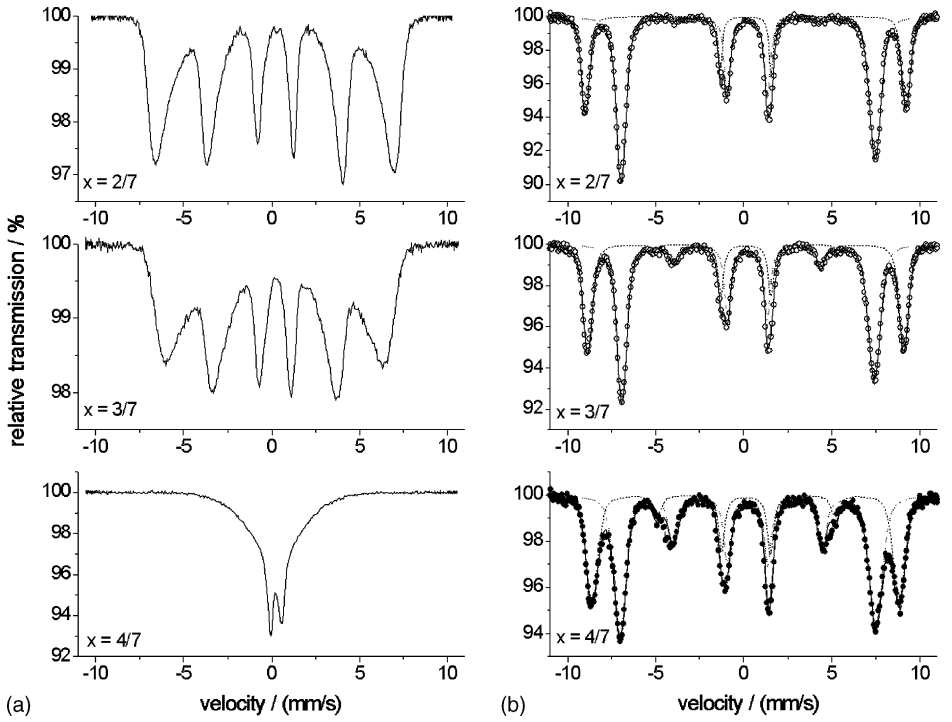

Fig. 7. Mössbauer spectra of samples $[Li_xMn_{1+x}Fe_{2-2x}O_4]_7$: (a) at room temperature; (b) at 4.2 K, $B_{ext} = 6$ T.

ions, qualitative conclusion concerning the manganese ion distribution between A and B sites in dependence on x), the following cation distribution formulas can be assumed for the $[Li_xMn_{1+x}Fe_{2-2x}O_4]_7$ ferrite samples with $x = 2/7$, 3/7 and 4/7:

$$x = 2/7: \quad (Li_{1.04}Mn^{2+}_{2.81-\delta}Fe^{3+}_{3.15}Mn^{3+}_{\delta})_A[Li_{0.96}Fe^{3+}_{6.85}Mn^{3+}_{6-\delta}Mn^{2+}_{0.19+\delta}]_BO_{28} \quad (1)$$

$$x = 3/7: \quad (Li_{2.37}Mn^{2+}_{1.0-\delta}Fe^{3+}_{2.98}Mn^{3+}_{0.65+\delta})_A[Li_{0.63}Fe^{3+}_{5.02}Mn^{3+}_{8.35-\delta}Mn^{2+}_{\delta}]_BO_{28} \quad (2)$$

$$x = 4/7: \quad (Li_{4.0}Fe^{3+}_{2.37}Mn^{3+}_{0.63})_A[Fe^{3+}_{3.63}Mn^{3+}_{9.37}Mn^{4+}_{1.0}]_BO_{28} \quad (3)$$

It can be concluded that with the increase of x the Fe fraction on B sites decreases. Corresponding with the results of the FEFF8 calculation of the XANES spectra, the manganese fraction on B sites increases with increasing x. In spite of the preferred occupation of octahedral sites by manganese(III) the experimental results concerning the site occupation by Li and Fe ions can only be explained by a partial occupation also of tetrahedral sites by Mn^{3+} ($x = 3/7$, 4/7). On the other hand, there is also a distribution of manganese(II) over A and B sites ($x = 2/7$, 3/7) with a preference for tetrahedral sites. Besides, some further thermal equilibration of the site occupation, described by the factor δ, cannot be excluded. The value of δ should be small and depend on the conditions of synthesis. The synthesis of single phase spinels of the given compositions requires synthesis temperatures between 800 and 900 °C and a quick cooling process. Therefore, the experimentally determined site occupation is the equilibrium distribution at the synthesis temperature. This fact should explain the presence of some tetrahedral site Mn(III) in presence of

Table 3
Mössbauer parameters of the samples $[Li_xMn_{1+x}Fe_{2-2x}O_4]_7$

Sample (x)	Fe(A) (%)	Fe(B) (%)	B_{eff} (Fe on B sites) (T)	B_{eff} (Fe on A sites) (T)
2/7	31.5	68.5	44.75	56.51
3/7	37.3	62.7	44.44	55.72
4/7	39.5	60.5	45.05	54.11

Fe(A), Fe(B): fraction of Fe on A and B sites (from spectra at 4.2 K, 6 T); B_{eff}: average effective magnetic hyperfine field at the iron nuclei resulting from the hyperfine and external fields.

octahedral site Fe(III). Obviously, this distribution is also favoured in comparison with the existence of tetrahedral Mn^{2+} and octahedral Mn^{4+} (beside Mn^{3+}) formally formed by a process $Mn_{(tetrahedral)}{}^{3+} + Mn_{(octahedral)}{}^{3+} \rightarrow Mn_{(tetrahedral)}{}^{2+} + Mn_{(octahedral)}{}^{4+}$. The latter distribution cannot be excluded by the Mössbauer results, but the result of XANES should exclude it. For aqueous systems the coexistence of Mn^{2+} and MnO_2 is well known from Pourbaix diagrams [27]. On the contrary, simple solid manganese oxides only coexist in two neighbouring oxidation numbers of manganese. This can be calculated with thermodynamic data given in [28]. In all probability, this should be current also for manganese containing complex oxides.

With increasing manganese and lithium content, the Mössbauer spectra of the spinel ferrite samples measured at room temperature (Fig. 7a) show an increasing line broadening of the sextets with increasing x and components at lower hyperfine field values appear. This is due to the presence of progressively more different environments for the Fe ions on A and B sites caused by the replacement of Fe ions by Li and Mn ions with increasing x. The magnetic order in spinel ferrites is caused by a superexchange interaction between magnetic ions on A and B sites via oxygen. The A–B interaction is dominant. As the number of non-magnetic Li ions increases, the number of magnetic neighbours on A and B sites decreases. This results in a decrease of the magnetic A–B interaction and a decrease of the Curie temperature with increasing x. Further decrease in the magnetic interaction is caused by a spin canting especially for the magnetic ions on the B sites. This can be concluded from the non-vanishing second and fifth line in the B subspectrum at 4.2 K in an external magnetic field. The spin canting angle increases with growing x. For the sample with $x = 4/7$ a spin canting is also observed for the magnetic A ions.

4. Conclusions

From the results discussed above, it turns out that the thermal decomposition of homogeneous freeze-dried lithium manganese iron formates, followed by an annealing process with a defined $p(O_2)$–temperature regime is a suitable method for preparing single phase ferrites $Li_xMn_{1+x}Fe_{2-2x}O_4$ with $0 \leq x \leq 1$ at a relatively low temperature. The formation of crystalline phases begins already at about 400 °C, although the development of favourable magnetic properties requires a synthesis temperature between 800 and 900 °C.

From the results of the XANES measurements one can conclude that the $Li_xMn_{1+x}Fe_{2-2x}O_4$ samples contain Mn(II) and Mn(III) or Mn(III) and Mn(IV) for $x < 0.5$ or $x > 0.5$, respectively. The average valences of manganese determined from the edge shift of the Mn K-edge XANES spectra agree well with the expected values and the results of the chemical analysis. In spite of the preferred occupation of octahedral sites by manganese(III) the results of the Mössbauer investigation can only be explained by a partial occupation also of tetrahedral sites by Mn(III). The distribution is a result of some thermal equilibration at the synthesis temperature. There are no experimental signs for a simultaneous presence of manganese in three different oxidation states as discussed in [11] for the solid solutions $MnFe_2O_4$–$LiMnFeO_4$ [vi].

With the increase of x the portion of Li ions occupying tetrahedral sites increases and becomes 100% at about $x = 4/7$. This result of the XRD investigation can be confirmed by the FEFF8 calculation of the XANES spectra. The calculation allows the interpretation of the changes in the Mn K-edge XANES spectra in terms of the proposed site occupation.

An increase of M_S with the increase of x (expected for a preferred substitution of magnetic ions in tetrahedral sites by non-magnetic Li ions) is not observed. It should be prevented by the decreasing cooperative coupling effects due to the reduction of the iron content. The increasing influence of spin canting, especially for the magnetic ions on the B sites, correlates with the increasing difference between the experimental and calculated M_S values (see Table 1).

Generally, it can be concluded from the results given above that the combination of XRD-, XANES-, Mössbauer- and magnetic investigations can result in useful and manifold informations concerning the structure, cation distribution and properties of spinel ferrites.

References

[1] M. Sugimoto, J. Am. Ceram. Soc. 82 (1999) 269.
[2] A. Lloyd, Key Eng. Mater. 122–124 (1996) 175.
[3] M.M. Thackeray, A. de Kock, M.H. Rossouw, D. Liles, J. Electrochem. Soc. 139 (1992) 363.
[4] M.M. Thackeray, C.S. Johnson, J.T. Vaughey, N. Li, S.A. Hackney, J. Mater. Chem. 15 (2005) 2257.

[5] P.B. Braun, Nature (London) 170 (1952) 1123.
[6] F. Petit, M. Lenglet, Solid State Commun. 86 (1993) 67.
[7] E. Wolska, P. Piszora, J. Darul, W. Nowicki, Mater. Sci. Forum 378–381 (2001) 551.
[8] (a) E. Wolska, P. Piszora, K. Stempin, C.R.A. Catlow, J. Alloys Comp. 286 (1999) 203;
(b) E. Wolska, P. Piszora, et al. Mater. Sci. Forum 321–324 (2000) 796–801.
[9] E. Rios, Y.-Y. Chen, M. Gracia, J.F. Marco, J.R. Gancedo, J.L. Gautier, Electrochim. Acta 47 (2001) 559.
[10] G. Bonsdorf, H. Langbein, K. Schäfer, Eur. J. Solid State Inorg. Chem. 34 (1997) 1051.
[11] R.G. Zakharov, R.F. Garbanov, Dokl. Akad. Nauk. 261 (1981) 633.
[12] H. Shigemura, H. Sakaebe, H. Kageyama, H. Kobayashi, A.R. West, R. Kanno, S. Morimoto, S. Nasu, M. Tabuchi, J. Electrochem. Soc. 148 (2001) A730.
[13] C. Wende, H. Langbein, Cryst. Res. Technol. 41 (2006) 18.
[14] T. Roisnel, J. Rodriguez-Carvajal, Mater. Sci. Forum (EPDIC 7) 378–381 (2001) 118.
[15] M. Lemonnier, O. Collet, C. Depautex, J.M. Esteva, R. Raoux, Nucl. Instrum. Meth. A 152 (1978) 10.
[16] H. Modrow, S. Bucher, J. Hormes, R. Brinkmann, H. Boennemann, J. Phys. Chem. B 107 (2003) 3684.
[17] A.L. Ankudinov, B. Ravel, J.J. Rehr, S.D. Conradson, Phys. Rev. B 55 (1998) 7565.
[18] H. Modrow, S. Bucher, J.J. Rehr, A. Ankudinov, Phys. Rev. B 67 (2003) 035123/1.
[19] K.H. Hallmeier, L. Uhlig, R.J. Szargan, J. Electron Spectrosc. Relat. Phenom. 122 (2002) 91.
[20] A. Pantelouris, H. Modrow, M. Pantelouris, J. Hormes, D. Reinen, Chem. Phys. 300 (2004) 13.
[21] B. Gilbert, B.H. Frazer, A. Belz, P.G. Conrad, K.H. Nealson, D. Haskel, J.C. Lang, G. de Stasi, J. Phys. Chem. A 107 (2003) 2839.
[22] K. Angermund, M. Bühl, U. Endruschat, F.T. Mauschik, R. Mörtel, R. Mynott, B. Tesche, N. Waldöfner, H. Bönnemann, G. Köhl, H. Modrow, J. Hormes, E. Dinjus, F. Gassner, H.-G. Haubold, T. Vad, J. Phys. Chem. B 107 (2003) 7507.
[23] A.L. Ankudinov, J.J. Rehr, J. Low, S. Bare, Phys. Rev. Lett. 86 (2001) 1642.
[24] A. Reich, M. Panthöfer, H. Modrow, U. Wedig, M. Jansen, J. Am. Chem. Soc. 126 (2004) 14428.
[25] S. Krupicka, Physik der Ferrite und der verwandten magnetischen Oxide, F. Vieweg + Sohn, Braunschweig, 1967.
[26] M.M. Thackeray, A. de Kock, W.F. David, Mat. Res. Bull. 28 (1993) 1041.
[27] D. Macdonald, Corros. Sci. 16 (1976) 461.
[28] I. Barin, Thermochemical Data of Pure Substances, VCH Verlagsgesellschaft mbH, Weinheim, 1993.